Review

Chemically imaging living cells by scanning electrochemical microscopy

Allen J. Bard*, Xiao Li, Wei Zhan

Department of Chemistry and Biochemistry, The University of Texas at Austin, Austin, TX 78712, United States

Abstract

Scanning electrochemical microscopy (SECM) is useful in probing and characterizing interfaces at high resolution. In this paper, the general principles of this technique are described and several applications of SECM to biological systems, particularly to living cells, is discussed, along with several example systems. Thiodione was detected and monitored electrochemically during the treatment of hepatocytes with cytotoxic menadione. The antimicrobial effects of silver(I) was followed by SECM through bacterial respiration. Living HeLa cells were shown to accumulate ferrocencemethanol (FcMeOH) and generated positive feedback for FcMeOH oxidation that can be further used to monitor the cell viability. Finally, individual giant liposomes, as cell models, with encapsulated redox compounds were successfully probed by SECM. In general SECM has the advantage of very high spatial resolution and versatility, especially for the detection of electroactive substances.
© 2006 Elsevier B.V. All rights reserved.

Keywords: Chemically imaging; Living cells; Scanning electrochemical microscopy

Contents

1. Introduction

The ideal biosensor is usually characterized as being robust, selective, reproducible and sensitive (with a large dynamic range). If it is to be used to characterize complete biological systems, like cells, when coupling and synergies can be probed, it should also show good temporal and spatial resolution.

We describe here the principles of scanning electrochemical microscopy (SECM), which has already found many appli-

cations in characterizing many different kinds of systems (e.g. electrode surfaces, liquid/liquid interfaces and biological samples), including surface structures in liquid environments with micrometer and nanometer resolution (Bard and Mirkin, 2001). SECM combines the virtues of electrochemistry at very small electrodes (ultramicroelectrodes), such as minimization of uncompensated resistance and capacitive effects, with those of an adjustable thin layer cell. The latter twin-electrode aspect of SECM allows one to make steady-state measurements of the type previously carried out with the rotating ring–disk electrode, but with considerably greater ease in fabrication and with comparable mass transfer rates, without the requirement of forced convection. Moreover, the theory of SECM is well-developed

---

* Corresponding author. Tel.: +1 512 471 3761; fax: +1 512 471 0088.
  E-mail address: asn@mail.utexas.edu (A.J. Bard).

with several different computer simulation methods described, so that one can utilize the current–distance (approach) curves above a substrate to obtain the distance between tip and surface with high accuracy as well as quantitative kinetic information about surface processes or reactions in solution. SECM is also useful for imaging and studying the uptake or release of chemical species from a surface (chemical imaging) and described below for processes in cells. Through monitoring the behavior of electrochemically active species, SECM generates real-time information with high spatial resolution, selectivity and versatility. In this paper, we will briefly describe the principles and practice of SECM. We then discuss its application to studies of the intake and efflux of material from bacterial and mammalian cells. We conclude with preliminary studies of using SECM to probe inside of cells.

2. Principles of the scanning electrochemical microscope

SECM is different than other scanning probe methods, like scanning tunneling and atomic force microscopy, in that it uses well-developed electrochemical methods to probe, quantitatively, the chemistry of a system. The technique is based on the measurement of the current through an ultramicroelectrode (UME) (an electrode with a radius, a, usually on the order of 1–25 μm) when it is held or moved in a solution in the vicinity of a substrate. For a conductive disk of radius a in an insulating sheath, this steady-state diffusion-controlled current when the tip is far from a surface is given by:

$$i_{T,\infty} = 4nFDca \qquad (1)$$

where D is the diffusion coefficient of species O, c, its concentration, n, the number of electrons passed per mole of O and F is the Faraday's constant. The current at electrodes with other shapes, e.g. hemispheres or cones, can be expressed in a similar way. The current is also relatively independent of the radius of the insulating sheath, r_g, often expressed in the SECM literature as RG $= r_g/a$. Moreover, because the flux of O to a small disk by diffusion, which is $\sim Dc/a$, is quite large, the current is relatively immune to convective effects like stirring in the solution. The current at a small disk also reaches steady state in a relatively short time ($\sim a^2/D$). For example, a 10 μm radius disk will attain steady state in a fraction of a second. These characteristics imply that an ultramicroelectrode used as a scanning tip and moved in a solution can be treated as an electrode whose current has attained steady state. Finally, because of the small currents that characterize most experiments with UME tips, generally pA to nA, resistive drops in the solution during passage of current are generally negligible.

Substrates, which can be solid surfaces of different types (e.g. glass, metal, polymer and biological material) or liquids (e.g. mercury and immiscible oil), perturb the electrochemical response of the tip when it is near the surface and this response provides information about the nature and properties of the substrate. The development of SECM depended on previous work on the use of UMEs in electrochemistry and the application of piezoelectric elements to position a tip, as in scanning tunnel-

ing microscopy (STM). Certain aspects of SECM behavior also have analogies in electrochemical thin layer cells and arrays of interdigitated electrodes.

The movement of the tip is usually carried out by drivers based on piezoelectric elements, similar to those used in STM. Typically inchworm drivers or stepping motors are used, since they can move larger distances than simple piezoelectric tube scanners. However, when higher resolution is needed, piezoelectric pushers can be added so that the inchworms and motors provide "coarse" drives and the pushers give nm resolution. Generally, the direction normal to the substrate is taken as the z-direction, while x and y are those in the plane of the substrate.

There are several modes of operation of the SECM. In the tip generation–substrate collection (TG/SC) mode, the tip is used to generate a reactant that is detected or reacts at a substrate. For example, the reaction O $+ ne \rightarrow$ R occurs at the tip and the reverse reaction occurs at the substrate. This mode of operation is similar to that at the rotating ring–disk electrode. Similar behavior is seen with a pair of side-by-side microband electrodes and in thin layer cells. An alternative mode, where the substrate is the generator and tip the collector (SG/TC mode) can also be employed and used to detect species formed at the substrate. The SG/TC mode was first used to study concentration profiles near an electrode surface without scanning and imaging and the feedback effects described below (Engstrom et al., 1986, 1987, 1988).

A frequent mode of operation of the SECM is the feedback mode, where only the tip current is monitored. Here, the tip current is perturbed by the presence of a substrate at close proximity by blockage of the diffusion of solution species to the tip (negative feedback) and by regeneration of O at the substrate (positive feedback). This effect allows investigation of both electrically insulating and conducting surfaces and makes possible imaging of surfaces and the reactions that occur there. This mode of operation with surface imaging was first described, along with the apparatus and theory, in a series of papers (Bard et al., 1989; Kwak and Bard, 1989a,b). The general principles of the feedback mode are shown in Fig. 1. As shown in Eq. (1), the current, $i_{T,\infty}$, is measured at the ultramicroelectrode tip when it is far from any surface (A) and the subscript, ∞, implying this long distance. In fact, long distance effects are seen when this distance is only a few tip diameters. The current under these conditions is driven by the hemispherical flux of species O from the bulk solution to the tip (Fig. 1A). When the tip is brought near an electrically insulating substrate, like a piece of glass or inert membrane (Fig. 1C), the substrate blocks some of the diffusion of O to the tip and the current will decrease compared to $i_{T,\infty}$. The closer the tip gets to the substrate, the smaller i_T becomes. At the limit when the distance between tip and substrate, d, approaches zero, i_T also approaches zero. This decrease in current with distance is called *negative feedback*. When the tip is brought near an electrically conductive substrate, like a piece of platinum or an electrode, while there is still blockage of diffusion of O to the tip by the substrate, there is also the oxidation of the product R back to O. This O generated at the substrate diffuses to the tip and causes an increase in the flux of O compared with $i_{T,\infty}$. Thus, with a conductive substrate $i_T > i_{T,\infty}$. In the limit as d approaches zero,
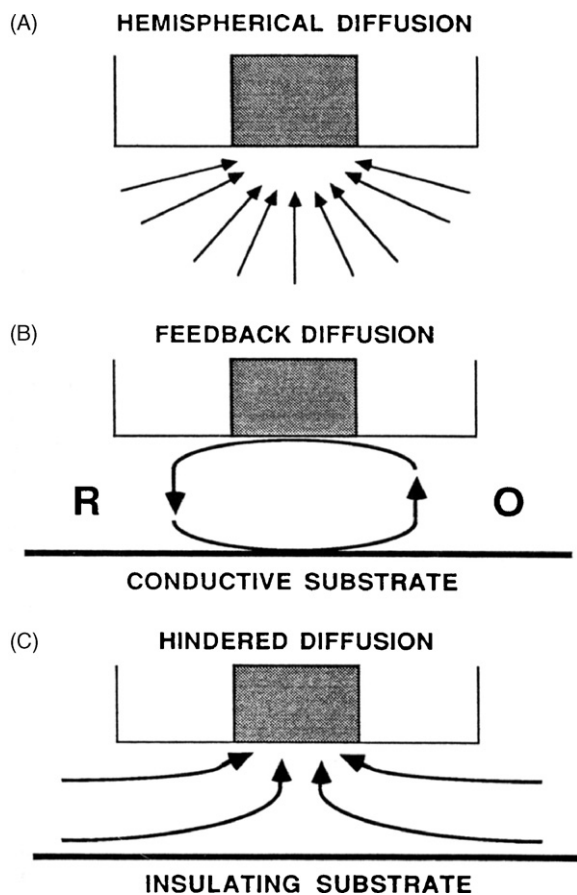
Fig. 1. (A) Diffusion to tip far from surface, (B) positive feedback at conductive surface and (C) negative feedback at insulating surface.

Fig. 2. Normalized approach curves I_T ($=i_T/i_{T,\infty}$) vs. L ($=d/a$) for: (A) conductive and (B) insulating substrate.

the tip will move into a regime where electron tunneling can occur and the tip current will get very large. This increase of current with decreasing distance is called *positive feedback*. A plot of i_T versus d, as a tip is moved in the *z*-direction is called an *approach curve*.

A quantitative description of approach curves can be obtained by solving the diffusion equations for the situation of a disk electrode and a planar substrate (Kwak and Bard, 1989a,b). Typical approach curves for a conductive substrate (essentially infinite rate of regeneration of O from R) and an insulating substrate (zero rate of regeneration of O) are shown in Fig. 2. These curves are given in dimensionless form by plotting $I_T = i_T/i_{T,\infty}$ (the tip current normalized by the current far from substrate) versus $L = d/a$ (the tip–substrate separation normalized by the tip radius). Since this plot involves only dimensionless variables, it does not depend upon the concentration or diffusion coefficient of O. From these curves one can readily find d from the measured I_T and a knowledge of a. The approach curves for an insulator actually also depend upon r_g, since the sheath around the conducting portion of the electrode also blocks diffusion, but this effect is not usually important with most practical tips. Note that while SECM has some characteristics in common with other scanning probe methods, like STM, it has the advantage of allowing one to determine, quite accurately, the distance between tip and substrate. Its response also depends upon well-
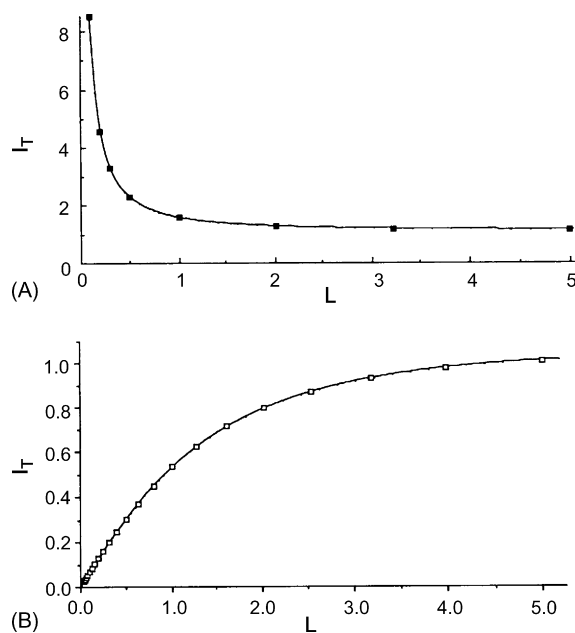
defined chemical reactions at the tip rather than resulting from tunneling.

By scanning the tip in the *x–y* plane and measuring current changes (the *constant height mode*) (or, less frequently, by maintaining a constant current and measuring the changes in d in a *constant current mode*) one can obtain topographic images of conducting and insulating substrates. The resolution of such images is governed by the tip radius, a, and d. Of particular interest is the use of SECM to perform "chemical imaging", and note differences in reaction rates at different locations on a surface. This mode is useful in studying biological materials (e.g. living cells) and surfaces that have active and passive sites.

3. SECM investigations of cells

A number of electrochemical methods have been developed to study processes occurring in biological systems. For example, Adams (1976) showed many years ago that microelectrodes could be used to detect neurotransmitters in the brain, and this type of research continues in a number of laboratories (e.g. Wightman et al., 1991a,b; Cannon et al., 2000). This work has led to a number of applications of microelectrodes to studies of cellular processes (Cooper and Jung, 2001; Gao et al., 2006, and references therein). Single cell amperometry or voltammetry has focused on measuring the concentrations and monitoring the dynamic release of biologically important molecules such as catecholamines, insulin and anticancer drugs from living cells. In such experiments, a micrometer-sized UME is positioned in close proximity to a cell membrane and used to oxidize (or reduce) the molecules ejected from the cell to obtain information on cellular functions at single cell levels (Wightman et al., 1991a,b; Ewing et al., 1992; Kennedy et al., 1993; Kuhr and Pantano, 1995; Lu and Gratzl, 1999).

SECM has also been used in studies of biological interest, e.g. in studies of enzymes and membranes, and to examine biological systems under physiological conditions with μm spatial resolution (Horrocks and Wittstock, 2000; Shiku et al., 2001). In the SECM measurements, the tip is scanned over the surface of a cell to obtain topographic images and maps of chemical reactivity across the cell surface. In this way, it has been used to image fluxes of oxygen at living cells and to obtain topographic images of various biological substrates (Lee et al., 1990; Tsionsky et al., 1997; Yasukawa et al., 1998, 1999). The photosynthetic and respiratory activities of single cells have been evaluated by monitoring the oxygen concentration profile around cells. The SECM based respiration activity measurements have been employed to build an anticancer drug sensitivity assay (Torisawa et al., 2004). SECM has also been used for imaging new emerging micron size topography and real-time detection of neurotransmitter secretion from living PC12, dopamine releasing immortal rat cells (Liebetrau et al., 2003; Hengstenberg et al., 2001). Potentiometric measurements employing scanning ion-selective microelectrodes have been demonstrated in the detection of calcium release at osteoclast cells that are responsible for the resorption of bone (Berger et al., 1999). Studies have also been undertaken to study the kinetics of transmembrane charge transfer in mammalian cells and in bacteria (Liu et al., 2000; Cai et al., 2002). The permeation of the nuclear membrane in the *Xenopus* oocyte by various mediators has also been studied (Guo and Amemiya, 2005).

We describe below several recent studies in our laboratory of the uptake and efflux of materials from living cells by SECM. We also describe early attempts at using SECM to penetrate cells and detect species inside the cells.

4. Menadione metabolism to thiodione in human liver cells

The cytotoxic effect of menadione on hepatocytes was investigated using the substrate generation/tip collection mode of SECM. Menadione has long been used to study oxidative stress in cells as it readily generates reactive oxidative species (ROS) that are harmful to biological systems. Because of its amphiphilic nature, menadione can diffuse into the cell without the assistance of transmembrane proteins or transport pumps (Cai et al., 2002; Liu et al., 2000; Yi and Gratzl, 1998). Once inside the cell, menadione is rapidly conjugated to intracellular glutathione via nucleophilic addition to form the stable conjugate thiodione. Thiodione can also generate ROS through redox reactions. Therefore, it must be removed from the intracellular space. Because the product thiodione is too hydrophilic to diffuse across the plasma membrane, an ATP-dependent pump is used for extracellular export. The loss of cell viability upon exposure to menadione is related to the depletion of glutathione within the cell, which occurs either through conjugating with menadione or through the oxidation of glutathione by forming a disulfide dimer (Di Monte et al., 1984; Duthie and Grant, 1989). Electrochemical studies have shown that even though glutathione is not electrochemically active on Pt electrode, the quinone moieties of both menadione and thiodione exhibit a

two-electron reduction at about −0.1 V versus NHE. The steady-state current of menadione is significantly larger than that of the thiodione because of its greater diffusion coefficient in aqueous solution. Although the reduction potential $E_{1/2}$ of thiodione is 150 mV more negative than that of menadione, this difference is not enough to distinguish between these two compounds using only their cyclic voltammograms (CV). However, thiodione shows an irreversible oxidation wave, ca. 0.74 V, where neither menadione nor glutathione exhibits electrochemical activity (Mauzeroll and Bard, 2004). Thus, both menadione and thiodione can be analyzed simultaneously using electrochemical methods.

The efflux of thiodione after the addition of menadione was studied with highly confluent liver cells adhering to the bottom of a Petri dish (Mauzeroll et al., 2004). A Pt UME with a radius of 10 μm was used to detect the thiodione concentration in solution by holding the tip at the potential for thiodione oxidation. The electrode was, ca. 100 μm away from a patch of cells. The concentration of thiodione can be easily calculated from the increasing anodic oxidation tip current by using the steady-state current equation for a CV at an UME. Shown in Fig. 3 is the dependence of thiodione concentration (black dots) in solution with time after the addition of 80 μM menadione. Generally, the concentration of thiodione increases with time and does not reach a steady state within the experimental time. The solid line is a non-linear fit of the concentration of thiodione in solution based on a constant flux model. In this model, it is assumed that the initial concentration of thiodione is zero at $t = 0$ when menadione is added, and the flux of thiodione J_{cell} from the cells is constant at $t > 0$. There is a time lag caused by the time needed for menadione uptake, conjugation and pump efflux processes. Overall, the experimental results match well with the calculation results, suggesting that the constant flux model can be used to describe the efflux of thiodione. Based on the model, the efflux
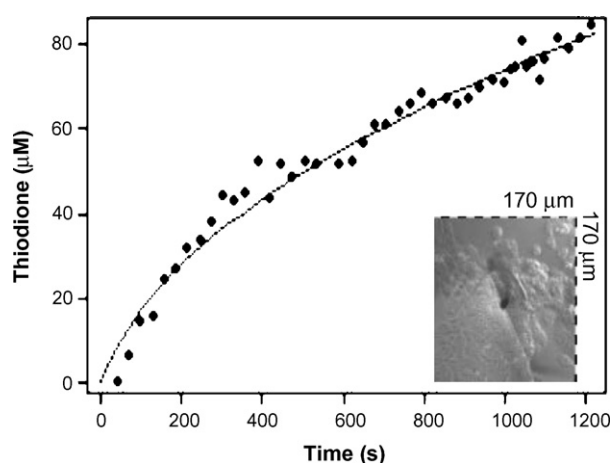

Fig. 3. Electrochemical detection of thiodione from highly confluent Hep G2 cells using 10 μm Pt UME. The potential was scanned in deoxygenated PBS buffer at 37.5 °C between −0.16 and 1.29 V vs. NHE at a scan rate of 100 mV/s. The concentration of thiodione in solution was calculated from the tip current at 1.14 V vs. NHE and plotted vs. time. The solid line is the non-linear simulation fitting based on a constant flux model. Inset shows the optical micrograph of 75–100% confluent liver cells used in these measurements and the black dot indicates the position of the Pt tip (Mauzeroll et al., 2004).

of thiodione is $4.7 \pm 0.3 \times 10^{-12}$ mol/cm^2 s for a highly confluent patch of cells. For each liver cell, the flux of thiodione is estimated to be 1×10^{-17} mol/cell s or 6×10^6 molecules/cell s. The general shape of this efflux is consistent with that observed in other studies, such as the doxorubicin export from Chinese hamster ovary cells (Chung et al., 1997; Lu and Gratzl, 1999).

The export of thiodione from isolated liver cells after addition of 80 μM menadione was also studied using SECM. First, menadione reduction was used to bring the electrode tip close to the cells in the *z*-direction perpendicular to the dish surface. Then, SECM images were recorded using a tip potential for the thiodione oxidation reaction while the tip was scanned in the *x*–*y* plane parallel to the dish bottom. Fig. 4A–D shows the successive SECM images from individual liver cells after addition of menadione. It took approximately 7 min to record each image. Fig. 4E and F are the optical images of the target liver cells using inverted microscopy. The dark disk in the micrograph is the 10 μm Pt UME used for the experiments. Fig. 4G–J shows the overlap between SECM and optical images. The varying position of liver cells in the SECM images is caused by some hysteresis in the inchworm during scanning. Optical images taken simultaneously can be used to correct for this hysteresis.

As shown in Fig. 4A, the oxidation current of thiodione observed when the tip is positioned above the liver cells is greater than that observed when the tip is positioned over the bare Petri dish. This current difference shows the higher concentration of thiodione close to the cells than in the bulk solution. In other words, the efflux of thiodione is only detected in the vicinity of the liver cells. As seen in Fig. 4A–D, the yellow color above the cells decreases with time, which indicates that the efflux of thiodione from the cells decreases with time. As all the images were taken from the same cells with the same tip–substrate distance, this behavior can be correlated to the fact that 80 μM menadione
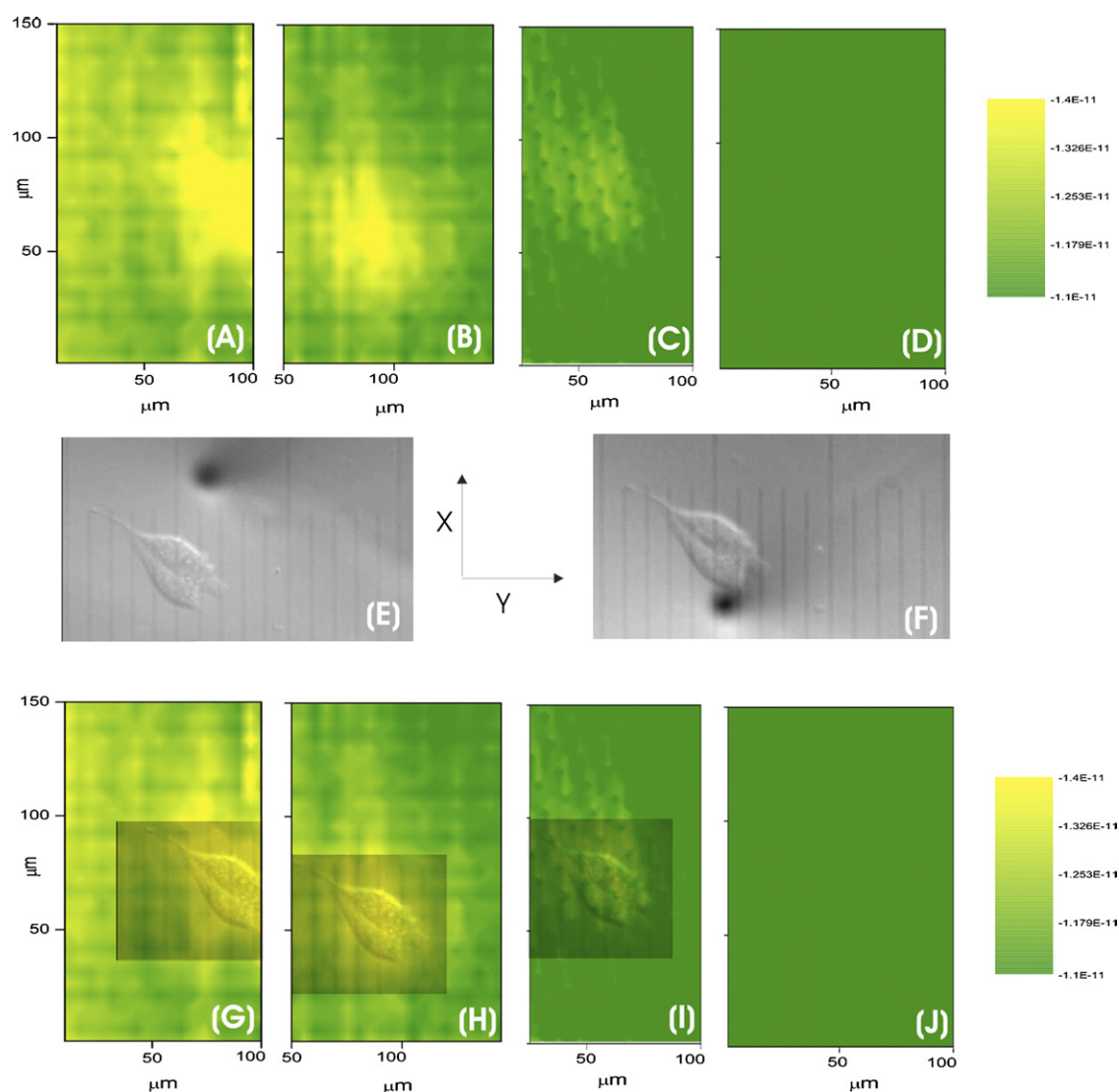

Fig. 4. Time-dependent profile of the export of thiodione from human liver cells using SECM. (A–D) SECM images of the Hep G2 cells with the tip potential at 1.19 V vs. NHE and scan rate of 150 μm/s. The distance between the tip and dish bottom is 4.3 μm. (E) and (F) are the optical images of the cells. The micrograph of the 10 μm Pt UME at different positions is indicated by the black dots. Each small division corresponds to 10 μm. (G–J) Superimposed optical micrograph on SECM images. All images were normalized with respect to scale (Mauzeroll et al., 2004).

is toxic to the cells and kills them within about 1 h in agreement with the cytotoxicity measurements (Mauzeroll et al., 2004).

5. SECM investigation of Ag⁺ interaction with respiratory chain of *Escherichia coli* (**Holt and Bard, 2005**)

Submillimolar concentrations of AgNO₃ are lethal to a range of bacterial species, both Gram-positive and Gram-negative (Bragg and Rainnie, 1974; Ghandour et al., 1988; Schreurs and Rosenberg, 1982; Yudkin, 1937); however, the mode of action is unknown. One possibility is that Ag⁺ uncouples the respiratory chain from oxidative phosphorylation (Schreurs and Rosenberg, 1982), causing a collapse in the proton motive force across the cytoplasmic membrane (Dibrov et al., 2002), for example, by interacting with thiol groups of membrane-bound enzymes and proteins (Liau et al., 1997; Zeiri et al., 2004). Again, it is unclear whether there is one major site of action or whether the silver(I) interacts detrimentally with the cell at many sites. Using SECM and several other electrochemical techniques, we studied the antibacterial effects of silver(I) ion on *E. coli*.

Respiration in the presence of glucose was measured using a Clark ultramicroelectrode (Carano et al., 2003) to determine oxygen concentration as a function of time. Fig. 5 shows schematically the electrode was assembled from a disk Pt microelectrode, a silver paint layer and a gas-permeable polymer membrane (high density polyethylene, HDPE). The membrane prevents the deactivation of the Pt electrode surface by adsorption of biological molecules. In addition, any contact between the
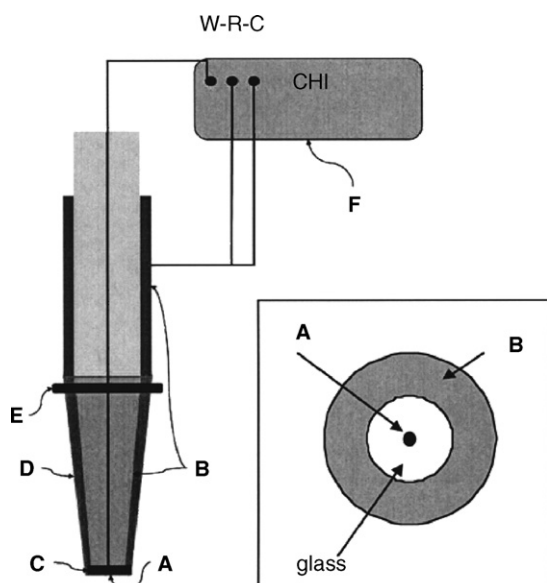
bacteria and the outer silver coating of the electrode is prevented. However, the extent of dissolution of the silver coating was sufficiently negligible to produce no appreciable concentration of Ag⁺ in the solution. In contrast to a Clark electrode of more traditional dimensions, the ultramicroelectrode draws currents in the nanoampere range. Not only can the ultramicroelectrode be used to undertake measurements in much smaller volumes (10–1000 μL) due to its small dimensions, but the formation of concentration gradients at the electrode/solution interface is also negligible in contrast to larger electrodes, so it rapidly attains a steady state without the necessity for convective mixing.

Measurements were made with a Clark ultramicroelectrode to monitor the oxygen reduction current in 1 mL solution of 0.1 M NaNO₃ and 0.1 M glucose containing 5×10^9 suspended bacteria. At $t = 12$ min, AgNO₃ was added to produce different concentrations of Ag⁺ (1–10 μM) to the normally respiring *E. coli* solutions and the change in respiration rate compared to that containing 0 μM Ag⁺ was measured. As shown in Fig. 6, the rate of respiration increased initially (as evidenced by the increased oxygen depletion) on the addition of silver(I) due to the uncoupling of the respiratory chain, followed by cessation of respiration. For 1 and 5 μM Ag⁺, there was a rapid increase in the rate of oxygen depletion, indicating an increase in bacterial respiration rate. For 10 μM Ag⁺ this period of stimulated respiration was not observed, and instead there was an immediate increase in the solution oxygen concentration due to cessation of respiration coupled with dissolution of oxygen from the atmosphere. The stimulated respiration observed on addition of Ag⁺ to bacteria has been noted previously (Bragg and Rainnie, 1974; Yudkin, 1937). The same effect is reported for rabbit brain mitochondria, along with an uncoupling of respiration from ATP synthesis (Silver, 2001).

Another way to probe bacterial respiration is to detect oxygen uptake by immobilized cells with an ultramicroelectrode posi-
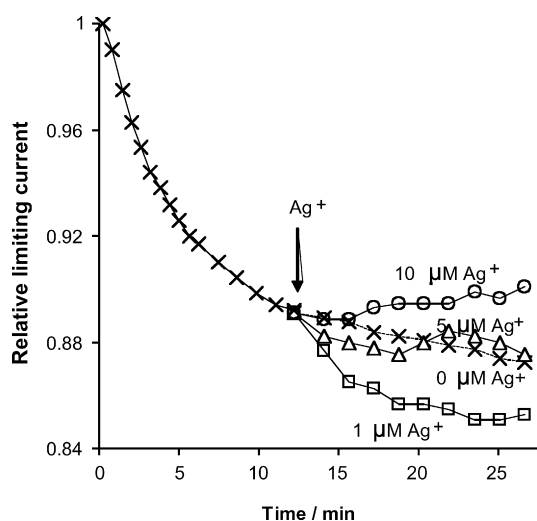
Fig. 5. Schematic diagram of membrane ultramicroelectrode based oxygen sensor (not to scale): (A) 25 μm diameter disk Pt working electrode encased in glass, (B) Ag layer acting as reference/counter electrode, (C) electrolyte film of 0.1 M, pH 7.0, PBS aqueous solution forming the electrolytic contact between working and reference electrodes, (D) 10 μm thickness HDPE membrane, (E) rubber O-ring and (F) power supply and electronic instrument for the measurements of the current output. Inset shows bottom view of electrode surface: (A) 25 μm Pt disk working electrode encased in glass and (B) Ag paint creating a ring reference/counter electrode (from Carano et al., 2003).

Fig. 6. Respiration of suspended *E. coli* in 1 mL solutions initially containing 0.1 M NaNO₃ and 0.1 M glucose, plotted as limiting current for oxygen reduction at −0.8 V vs. silver paint relative to limiting current at $t = 0$ min, as measured by Clark ultramicroelectrode. Crosses, 0 μM AgNO₃ added at $t = 12$ min; circles, 10 μM AgNO₃ added at $t = 12$ min; triangles, 5 μM AgNO₃ added at $t = 12$ min; squares, 1 μM AgNO₃ added at $t = 12$ min (from Holt and Bard, 2005).

tioned closely to an immobilized cell surface by SECM. There are several advantages to performing experiments in this manner compared to using cells suspended in solution: (1) experiments can be performed using fewer cells, in a smaller volume; (2) electrode surface fouling is minimized as the immobilized cells cannot adsorb to the surface of the electrode so that real-time silver uptake experiments can then be performed without having to remove the cells from solution by centrifugation prior to analysis; (3) the precise positioning of the electrode above the surface of the cells achievable through this method allows the extraction of more quantitative data and theoretical modeling of the uptake kinetics.

One example is shown in Fig. 7a, where the electrode was located 25 μm from the immobilized *E. coli*. A solution drop of 1 μM AgNO$_3$ in 0.1 M NaNO$_3$ was placed above the cells and the oxygen concentration measured over time. This same approach could be used with a Pt UME and stripping voltammetry to monitor Ag$^+$ uptake by recording silver depletion from
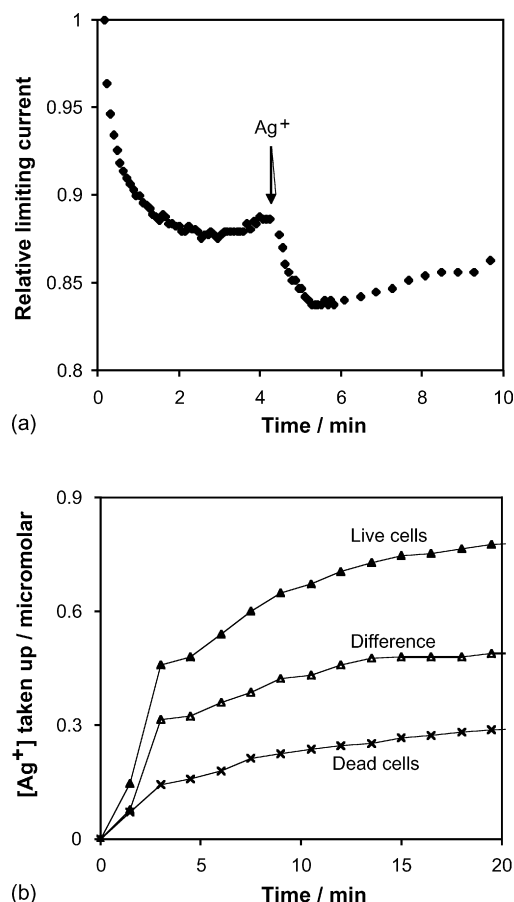
the region directly above the cells. Fig. 7b shows the total amount of silver(I) taken up by the live and dead *E. coli* (average of two experiments in each case). The data show that almost 0.3 μM of the Ag$^+$ was depleted by the dead cells after 20 min, presumably by interaction with functional groups on the outside of the cells. In contrast, the live cells consumed almost 0.8 μM of the 1 μM Ag$^+$ originally in solution. Most of this uptake took place within the first 10 min, with more gradual uptake thereafter. The difference in uptake between the dead and live cells (uptake live minus uptake dead) is also shown in Fig. 7b, and corresponds to the amount of Ag$^+$ accumulated *within* the live cells, rather than on the outside. This gives an approximate value of 0.5 μM for the concentration of silver transported into the cells after 20 min, corresponding to ∼60% of the total silver(I) depleted from solution.

These results demonstrate the applicability of SECM to studies of toxicity effects in bacteria in general and with various silver preparations that have been of interest because of their antibiotic properties. They also offer some insight into the mode of action of silver(I) in bacterial respiration processes.

6. HeLa cells activity probed using FcMeOH oxidation

While SECM has been widely applied to many biological systems, most applications used oxygen reduction to monitor the respiratory activity of cells. Fig. 8 shows SECM images of HeLa cells in an undearated culture medium containing 1 mM ferrocene methanol (FcMeOH). These images were obtained at a 10 μm Pt tip with the tip held at the potential for (a) O$_2$ reduction and (b) FcMeOH oxidation. The scan rate was 60 μm/s with the tip at a distance of 18 μm from the bottom of Petri dish. For comparison, the same group of HeLa cells was under investigation for these two SECM images.

When the tip potential is held at the potential for O$_2$ reduction, the current with the tip above HeLa cells is smaller (i.e. topographic color is darker green) than that of the background, as shown in Fig. 8a. The lower steady-state current for O$_2$ reduction when the tip is positioned above a HeLa cell is characteristic of negative feedback due to the O$_2$ uptake and respiration activities of HeLa cells, as well as to the blocking effect the cells have on O$_2$ diffusion (Kaya et al., 2003). Although O$_2$ reduction has long been used to monitor the viability of living cells, a drawback to this is the instability of O$_2$ reduction on Pt electrode reaction with time because of changes in the Pt surface. This can sometimes be overcome by a superimposed potential profile that cleans the electrode. For example, as shown in Fig. 8a, the background color changes from yellow at the top left (starting point for the scan) to green at the bottom right of the image (end point), a 23% decrease of the background reduction current is observed for this image that is largely due to this continuous electrode deactivation.

Fig. 8b illustrates the use of FcMeOH as a mediator. When FcMeOH oxidation occurs at the tip, the current for the oxidation of FcMeOH is higher than background (i.e. color over HeLa cell is yellow). The positive feedback suggests that the HeLa cell below the tip can participate in the FcMeOH/FcMeOH$^+$ redox
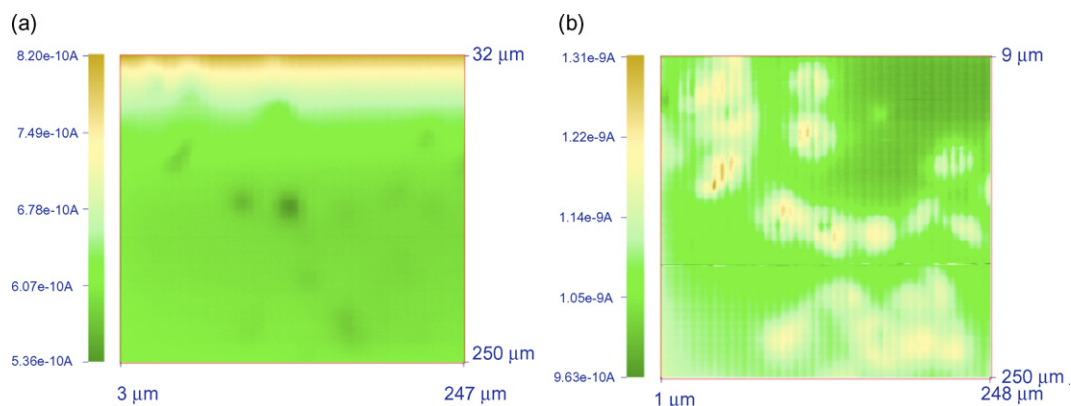

Fig. 7. (a) Limiting current for oxygen reduction, relative to that at *t* = 0, at −0.8 V vs. Ag paint, obtained at 25 μm Pt disc—Ag ring electrode located 25 μm above immobilized *E. coli* over time. Electrolyte initially was 10 μL drop of 0.1 M NaNO$_3$. At *t* = 4 min a 1 μL drop of 1 μM AgNO$_3$ was added. (b) Concentration of Ag$^+$ taken up by immobilized *E. coli*, measured using the stripping peak height obtained using a 25 μm Pt disc electrode located 1000 μm above the cells, held at −0.3 V vs. silver paint for 60 s before sweeping −0.3 to 0.35 V at 0.1 V/s to obtain stripping peak. Solid triangles, live cells; crosses, dead cells previously treated with 10 mM KCN for 2 h; open triangles, difference in Ag$^+$ taken up by dead and alive cells (from Holt and Bard, 2005).

Fig. 8. The SECM images of HeLa cells on Petri dish in culture medium containing 1 mM FcMeOH. The electrode is a 10 μm Pt UME with RG of 5. Scan rate is 60 μm/s while the electrode is held 18 μm away from the Petri dish bottom. The electrode potential is held at: (a) −0.3 V vs. NHE for O_2 reduction reaction and (b) 0.6 V vs. NHE for FcMeOH oxidation reaction. The rest time for O_2 reduction is 2 min while that of the FcMeOH oxidation is 15 s. The same group of HeLa cells was studied for both images (from Li and Bard, in preparation).

cycle between the tip and cell, i.e. HeLa cells can reduce the FcMeOH⁺ generated by the tip, which then diffuses back to the tip and leads to an increase in the oxidation current. Compared with the O_2 reduction reaction, oxidation of FcMeOH on a Pt UME was more stable. Thus, clear and reproducible images of HeLa cells can be easily obtained using FcMeOH as a mediator. Analogous feedback effects of some other electrochemically active mediators on cells has previously been observed with SECM, e.g. (Liu et al., 2001), where negative feedback was obtained for hydrophilic mediators like ferrocene carboxylate, while positive feedback was generated for hydrophobic ones, like menadione.

This positive feedback observed in the oxidation of FcMeOH over HeLa cells suggests a relationship between cell viability and positive feedback, which was then tested. Fig. 9a shows a sequence of SECM images of the same HeLa cells changing with time upon addition of 30 mM KCN, which kills these cells, to a culture medium containing 1 mM FcMeOH. FcMeOH oxidation at the tip was used to record the cell images. Pt UME was scanned at 60 μm/s in the x–y plane while the tip was 15 μm away from the dish bottom. Before the addition of CN⁻, the SECM image shows two yellow spots corresponding to the location of two living HeLa cells on the Petri dish. After 22 min following the CN⁻ addition, negative feedback is observed from the HeLa cell.
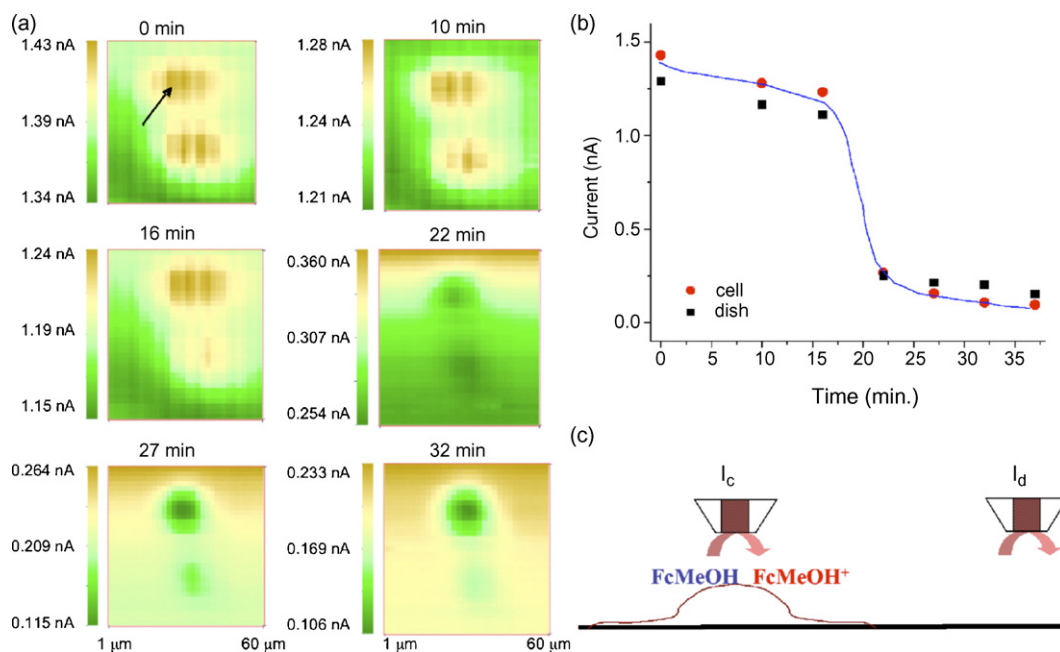

Fig. 9. (a) SECM images of HeLa cells upon addition of 30 mM KCN into a culture medium containing 1 mM FcMeOH. A 10 μm Pt electrode at the potential of 0.6 V vs. NHE was scanned at 60 μm/s. (b) Variation of current measured by SECM in (a) with time. I_d is the dish current while I_c is the cell current measured just above a HeLa cell. The distance between the electrode tip and the bottom of the Petri dish is 15 μm. The blue line is a guide for the eye. (c) A schematic graph for the dish current, I_d, and the cell current, I_c. The grey line outlines the shape of HeLa cell on the Petri dish indicated by the black line. The Red curved arrow indicates the oxidation reaction occurring on the electrode (from Li and Bard, in preparation). (For interpretation of the references to color in this figure legend, the reader is referred to the web version of the article.)

Fig. 9b shows variation of the dish current (solid black squares) and cell current (solid red circles) measured by SECM upon the addition of 30 mM KCN. The blue line is a guide for the eye. Fig. 9c schematically shows the relative geometry for the dish current I_d and cell current I_c, where the dish current I_d is the current when the tip is above the bottom of the bare Petri dish next to a group of cells, while the cell current I_c is the current when the tip is directly above a HeLa cell. With the addition of KCN, both the dish current and the cell current decrease slowly with time for the first 15 min, while positive feedback is observed. At around 18 min, both currents decrease dramatically and negative feedback is observed. This negative feedback indicates the cessation of HeLa cell activity, and it is due to blocking effect by the dead HeLa cells on the dish bottom. The killing time around 20 min, matches well with previously reported results (Kaya et al., 2003). Note that the current far from the Petri dish bottom remains essentially constant throughout this period.

Cyanide ion is lethal for mammalian cells and bacteria, because it binds tightly to cytochrome oxidase and blocks electron transport in the respiration chain, thus decreasing uptake of oxygen by the cells. This experiment clearly suggests that the positive feedback of FcMeOH observed is due to the interaction of FcMeOH$^+$ with living HeLa cells. Dead cells do not generate positive feedback. Hence, the FcMeOH oxidation reaction can be used as an electrochemical indication to test the viability of HeLa cells.

To further test the interaction between FcMeOH and HeLa cells, an accumulation–leak test was performed. HeLa cells were first cultivated in a 2 mL culture medium containing 1 mM FcMeOH. After 2 h to allow the cells to accumulate FcMeOH, the culture medium was removed and the Petri dish with HeLa cells was rinsed several times to wash away FcMeOH possibly adsorbed on the dish surface and the surface of the cells. Then, 2 mL fresh culture medium without FcMeOH was added to the Petri dish. SECM experiments were performed to measure the change of FcMeOH oxidation current in solution due to its efflux from the HeLa cells. Fig. 10 shows the variation of dish currents I_d (black squares with error bar) and cell current I_c (red squares with error bar) with time after the change of culture medium. As stated above, the dish current indicates the local concentration of FcMeOH around the tip. The cell current is directly related to the interaction between the tip and the cell below. Because of the interaction, the cell current is always larger than the dish current. Shown in Fig. 10, both currents increased rapidly with time within the first 40 min. After 90 min, the currents gradually reached a plateau.

For a more quantitative understanding of the feedback experiments, a model based on the finite difference method (FDM) was adopted to simulate the cross membrane diffusion processes of FcMeOH (Li and Bard, in preparation). The dish current was modeled by four successive processes: diffusion within the cell, diffusion across the membrane, diffusion in solution and accumulation in hydrophobic region within the cell. Shown in Fig. 10, the solid black line is the variation of simulated dish current with time. The simulation uses the known diffusion coefficient of FcMeOH in aqueous solution, 7×10^{-6} cm^2/s. From the sim-
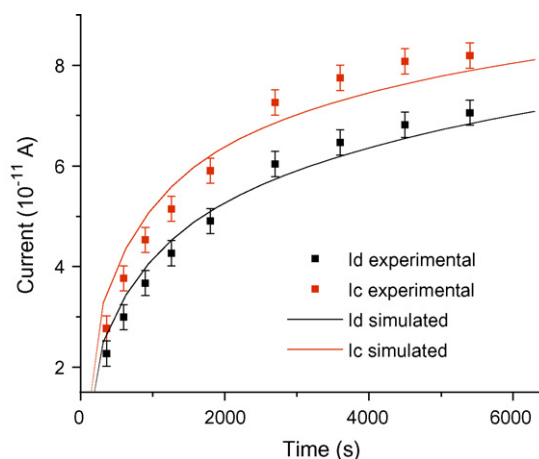

Fig. 10. Variation of the dish current (black squares with error bar) and the cell current (red squares with error bar) measured by SECM during accumulation–leaking experiments with time. I_b is the dish current while I_c is the cell current. A 10 μm Pt electrode at the potential of 0.6 V vs. NHE was scanned at 180 μm/s and held at 18 μm away from the dish bottom. The solid lines are the simulated dish current (black) and cell current (red) using the finite difference method on a surface reduction model. Details about the simulation are described in Li and Bard (in preparation). (For interpretation of the references to color in this figure legend, the reader is referred to the web version of the article.)

ulation, the diffusion coefficient of FcMeOH across the plasma membrane was estimated to be in the order of 3.8×10^{-6} cm/s, while of FcMeOH accumulates within the hydrophobic region of the cell. For the dish current simulation, two mechanisms were tested. In one mechanism, FcMeOH$^+$ is heterogeneously reduced back to FcMeOH on the outer surface of the plasma membrane of the HeLa cells, while in the other FcMeOH$^+$ diffuses into the cell where it is homogenously reduced. The simulation results suggest that the cell current is mainly dependent upon the transmembrane diffusion of FcMeOH in the latter mechanism and this mechanism does not work for our tested system. Shown in Fig. 10, the solid red line is the simulated cell current using the first mechanism. These results suggest that FcMeOH oxidation provides an easy way to obtain clear and reproducible images of cells on a surface by SECM and to test cell viability.

7. SECM probing single giant liposomes containing Ru(bpy)$_3$$^{2+}$

In the above examples we have discussed how SECM can be used with the tip immediately outside of cells to monitor the transport of electrochemically active species across cell membranes. It would also be of interest to monitor redox processes and respiration directly *inside* biological cells. Considering the architectural and functional complexity of such cells, we thought it desirable to start with an analogous system of a simpler configuration where the structure and chemical content can be fully controlled. As shown in Fig. 11, we first used SECM to probe immobilized liposomes, which represent prototypical models for biological cells, and to obtain information about their behavior.
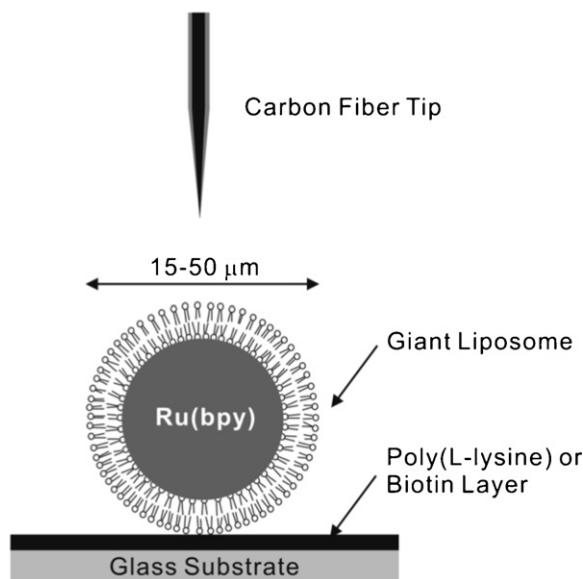
Fig. 11. Experimental setup. Liposomes of 15–50 μm were immobilized on glass substrates via either poly(L-lysine) or biotin–avidin–biotin sandwich structure; these liposomes were probed by a submicron-sized carbon fiber tip controlled by the SECM (from Zhan and Bard, 2006).
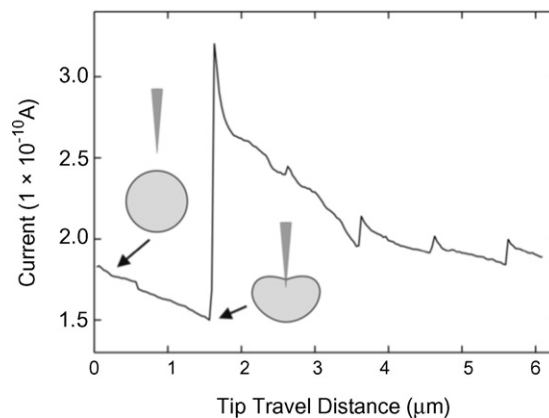

Fig. 12. SECM monitoring of tip current when it breaks through the bilayer(s) of $Ru(bpy)_3^{2+}$ containing liposomes. The tip potential was held at 1.2 V (vs. Ag QRE) where $Ru(bpy)_3^{2+}$ is oxidized to $Ru(bpy)_3^{3+}$. A 1 mM ferrocenylmethyl-trimethylammonium perchlorate ($FeCp_2TMA^+$) in Tris–HCl buffer (10 mM Tris and 0.1 M NaCl, pH 7.0) was used as the redox mediator (from Zhan and Bard, 2006).

To first test the concept with a simpler system, we have first studied giant liposomes encapsulated with redox molecules of interest (Zhan and Bard, 2006). Here, the good spatial control of the UME by SECM allows one to differentiate a mediator in the external aqueous medium with a different one that is encapsulated. SECM should also be useful in studies of chemical leakage from the liposome interior. Furthermore, SECM combined with sharp, submicrometer-sized electrodes allowed us to probe into liposomes and cells to obtain useful information.

Liposomes of various sizes and configurations have been made and studied, for example, as biomembrane and proto-cell models (New, 1990; Sackmann, 1995). Liposomes have also been pursued as biocompatible carriers and containers in biomedical and pharmaceutical applications. Indeed, many hydrophilic compounds, including drugs, enzymes and DNA, have been successfully encapsulated in liposomes (Lasic, 1998; Luisi and Walde, 2000). Giant liposomes, with diameters of a few microns and above, are particularly attractive systems because of their accessibility to optical microscopy and various micromanipulation techniques.

We developed a double-emulsion method to prepare giant liposomes containing $Ru(bpy)_3^{2+}$. To probe these liposomes immobilized on a glass substrate, we also prepared submicrometer carbon fiber electrodes. These small electrodes were further coated with electrophoretic paint and as a result, only the conical apex (tip) of electrodes was exposed and electrochemically active. This treatment produced a nanometer-sized tip that gave negative feedback when the tip was brought down to glass and liposome surfaces. To break through into the immobilized liposome, an approach curve was first obtained with a mediator like cationic ferrocenylmethyl-trimethylammonium perchlorate ($FeCp_2TMA^+$), where the tip was stopped when the current dropped to 85% of the steady-state tip current in the bulk ($i_{T,\infty}$).

This normally brought the tip down to less than 200 nm above the membrane surface (by fitting the experimental data with the approach curve model for conically shaped electrodes (Zoski et al., 2004). The tip was then further lowered into the cell, while held at the potential for $Ru(bpy)_3^{2+}$ (and $FeCp_2TMA^+$) oxidation as the current was monitored. A characteristic breakthrough curve is shown in Fig. 12. In this case, a decrease of current was first observed as the tip traveled down to the surface.

After the apex of the tip touched the membrane, a further lowering of tip deformed the lipid bilayers downward, accompanied by a further drop of the current. This effect is reminiscent of the SECM behavior noted when a tip approaches the interface between an aqueous solution and an immiscible liquid and a thin layer of solution is trapped (Wei et al., 1995). The breakthrough of the liposome normally took place a few micrometers below the point where the tip first touched the liposome surface, which varied from one experiment to another due to differences in the tip sharpness and liposome size. At the breakthrough point, a transient with a sharply rising current was obtained for the liposome, which represents the sudden immersion of the tip into a solution of a relatively high concentration of $Ru(bpy)_3^{2+}$ resulting in a potential step transient with some contribution from charging current.

We could also observe the encapsulated $Ru(bpy)_3^{2+}$ leaking out of a liposome after breakthroughs by continuously recording cyclic voltammograms inside. Shown in Fig. 13 are five CVs obtained in a time span of 20 min. Because of the existence of a concentration gradient inside/outside liposome, the current due to $Ru(bpy)_3^{2+}$ oxidation kept decreasing. By comparing the leakage rate of $Ru(bpy)_3^{2+}$ with a species of known concentration in the surrounding solution, we could estimate the concentration of the encapsulated material.

Individual redox encapsulated giant liposomes can also be probed by microelectrode tips to obtain useful information about molecular transport through the bilayer. This adds an alternative probe to those based on fluorescence and radioactivity in studying bilayer lipid membranes (BLMs). In comparison to
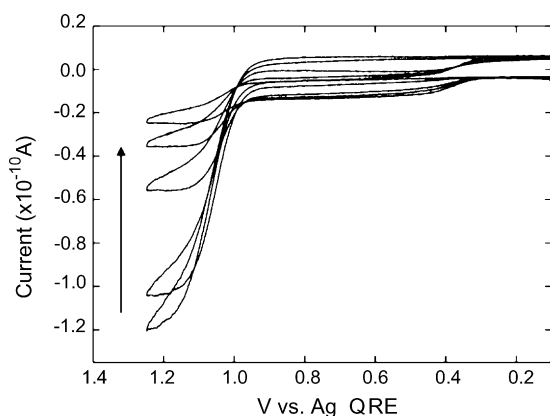
Fig. 13. Voltammetric responses of Ru(bpy)$_3^{2+}$ confined in a single giant liposome. The encapsulated Ru(bpy)$_3^{2+}$ leaked out of the liposome, as indicated by a decrease of the oxidation current along the arrow direction. Each CV was taken about 5 min after the previous one. Solution conditions are the same as those in Fig. 3 (from Zhan and Bard, 2006).

the BLM setup (Amemiya and Bard, 2000; Tsionsky et al., 1999) we previously used to study charge and ion transfer, the present system based on giant liposomes should allow one to perform similar measurements over a more extended period of time.

8. Conclusions

Previous work, as well as the studies outlined here, has demonstrated the utility and potential of SECM to studies of biological systems, including living cells. In particular, we showed: (1) thiodione was detected and monitored electrochemically during the cytotoxic process of menadione on hepatocytes; (2) antimicrobial effects of silver(I) was followed by SECM through bacterial respiration; (3) living HeLa cells accumulate FcMeOH and generate positive feedback for FcMeOH oxidation that can be further used to monitor the cell viability; (4) individual giant liposomes encapsulated with redox compounds were successfully probed by SECM. The technique has the advantage of very high spatial resolution and versatility, especially for the detection of electroactive substances. Selectivity and utilization for species that are not electroactive can be attained by modifying the tip, e.g. with enzymes (Bard and Mirkin, 2001).

References

Adams, R.N., 1976. Anal. Chem. 48, 1126A.
Amemiya, S., Bard, A.J., 2000. Anal. Chem. 72, 4940–4948.
Bard, A.J., Fan, F.-R.F., Kwak, J., Lev, O., 1989. Anal. Chem. 61, 132.
Bard, A.J., Mirkin, M.V. (Eds.), 2001. Scanning Electrochemical Microscopy. Marcel Dekker, New York.
Berger, C.E.M., Horrocks, B.R., Datta, H.K., 1999. Electrochim. Acta 44, 2677.
Bragg, P.D., Rainnie, D.J., 1974. Can. J. Microbiol. 20, 883–889.
Cai, C., Liu, B., Mirkin, M.V., Frank, H.A., Rusling, J.F., 2002. Anal. Chem. 74, 114.
Cannon, D.M., Winograd Jr., N., Ewing, A.G., 2000. Annu. Rev. Biophys. Biomol. Struct. 29, 239.
Carano, M., Holt, K.B., Bard, A.J., 2003. Anal. Chem. 75, 5071.

Chung, J.H., Seo, D.C., Chung, S.H., Lee, J.Y., Seung, S.A., 1997. Toxicol. Appl. Pharmacol. 142, 378.
Cooper, J.M., Jung, S.-K., 2001. In: Bard, A.J., Stratman, M., Wilson, G.S. (Eds.), Encyclopedia of Electrochemistry, vol. 9. Wiley-VCH, pp. 31–49.
Di Monte, D., Ross, D., Bellomo, G., Eklow, L., Orrenius, S., 1984. Arch. Biochem. Biophys. 235, 334.
Dibrov, P., Dzioba, J., Gosink, K.K., Hase, C.C., 2002. Agents Chemother. 46, 2668–2670.
Duthie, S.J., Grant, M.H., 1989. Biochem. Pharmacol. 38, 1247.
Engstrom, R.C., Meaney, T., Tople, R., Wightman, R.M., 2005. Anal. Chem. 59.
Engstrom, R.C., Weber, M., Wunder, D.J., Burgess, R., Winquist, S., 1986. Anal. Chem. 58, 844.
Engstrom, R.C., Wightman, R.M., Kristensen, E.W., 1988. Anal. Chem. 60, 652.
Ewing, A.G., Strein, T.S., Lau, Y.Y., 1992. Acc. Chem. Res. 25, 440.
Gao, N., Zhao, M., Zhang, X., Jin, W., 2006. Anal. Chem. 78, 231.
Ghandour, W., Hubbard, J.A., Deistung, J., Hughes, M.N., Poole, R.K., 1988. Appl. Microbiol. Biotechnol. 28, 559–565.
Guo, J., Amemiya, S., 2005. Anal. Chem. 77, 2147.
Hengstenberg, A., Blöchl, A., Dietzel, I.D., Schuhmann, W., 2001. Angew. Chem. Int. Ed. 40, 905.
Holt, K.B., Bard, A.J., 2005. Biochemistry 44, 13214.
Horrocks, B.R., Wittstock, G., 2000. Scanning Electrochemical Microscopy. Marcel Dekker, New York, pp. 445–519.
Kaya, T., Torisawa, Y.-S., Oyamatsu, D., Nishizawa, M., Matsue, T., 2003. Biosens. Bioelectron. 18, 1379.
Kennedy, R.T., Huang, L., Atkinson, M.A., Dush, P., 1993. Anal. Chem. 65, 1882.
Kuhr, W.G., Pantano, P., 1995. Electroanalysis 7, 405.
Kwak, J., Bard, A.J., 1989a. Anal. Chem. 61, 1794.
Kwak, J., Bard, A.J., 1989b. Anal. Chem. 61, 1221.
Lasic, D.D., 1998. TIBTECH 16, 307–321.
Lee, C.M., Kwak, J.Y., Bard, A.J., 1740. Proc. Natl. Acad. Sci. U.S.A. 87.
Li, X., Bard, A.J., in preparation.
Liau, S.Y., Read, D.C., Pugh, W.J., Furr, J.R., Russell, A.D., 1997. Lett. Appl. Microbiol. 25, 279–283.
Liebetrau, J.M., Miller, H.M., Baur, J.E., Takacs, S.A., Anupunpisit, V., Garris, P.A., Wipf, D.O., 2003. Anal. Chem. 75, 563.
Liu, B., Cheng, W., Rotenberg, S.A., Mirkin, M.V., 2001. J. Electroanal. Chem. 500, 590.
Liu, B., Rotenberg, S.A., Mirkin, M.V., 2000. Proc. Natl. Acad. Sci. U.S.A. 97, 9855.
Lu, H., Gratzl, M., 1999. Anal. Chem. 71, 2821.
Luisi, P.L., Walde, P., 2000. Giant Vesicles, vol. 6. John Wiley & Sons Ltd., New York.
Mauzeroll, J., Bard, A.J., 2004. Proc. Natl. Acad. Sci. U.S.A. 101, 7862.
Mauzeroll, J., Bard, A.J., Owhadian, O., Monks, T.J., 2004. Proc. Natl. Acad. Sci. U.S.A. 101, 17582.
New, R.R.C., 1990. Liposomes: A Practical Approach. Oxford University Press, Oxford, England.
Sackmann, E., 1995. In: Lipowsky, R., Sackmann, E. (Eds.), Structure and Dynamics of Membranes: From Cells to Vesicles. Elsevier Science B.V., Amsterdam, The Netherlands, pp. 1–63.
Schreurs, W.J.A., Rosenberg, H., 1982. J. Bacteriol. 152, 7–13.
Shiku, H., Ohya, H., Matsue, T., 2001. In: Bard, A.J., Stratmann, M. (Eds.), Encyclopedia of Electrochemistry, vol. 9. Wiley-VCH, pp. 257–275.
Silver, S., 2001. FEMS Microbiol. Rev. 27, 341–353.
Torisawa, Y., Shiku, H., Kasai, S., Nishizawa, M., Matsue, T., 2004. Int. J. Cancer 109, 302.
Tsionsky, M., Cardon, Z.G., Bard, A.J., Jackson, R.B., 1997. Plant Physiol. 113, 895.
Tsionsky, M., Zhou, J., Amemiya, S., Fan, F.-R., Bard, A.J., Dryfe, R.A.W., 1999. Anal. Chem. 71, 4300–4305.
Wei, C., Bard, A.J., Mirkin, M.V., 1995. J. Phys. Chem. 99, 16033–16042.
Wightman, R.M., Jankowski, J.A., Kennedy, R.T., Kawagoe, K.T., Schroeder, T.J., Leszczyszyn, D.J., Near, J.A., Diliberto Jr., E.M., Viveros, O.H., 1991a. Proc. Natl. Acad. Sci. U.S.A. 88, 10754.
Wightman, R.M., Kennedy, R.T., Wiedemann, D.J., Kawagoe, K.T., Zimmerman, J.B., Leszczyszyn, D.J., 1991b. In: Montenegro, M.I., Queirós, M.A.,

Daschbach, J.L. (Eds.), Biological Systems in Microelectrodes: Theory and Applications. Kluwer Academic Publishing, Dordrecht, pp. 453–462.

Yasukawa, T., Kaya, T., Matsue, T., 1999. Anal. Chem. 71, 4637.

Yasukawa, T., Kondo, Y., Uchida, I., Matsue, T., 1998. Chem. Lett. 27, 767.

Yi, C., Gratzl, M., 1998. Biophys. J. 75, 2255.

Yudkin, J., 1937. Enzymologia 2, 161–170.

Zeiri, I., Bronk, B.V., Shabtai, Y., Eichler, J., Efrima, S., 2004. Appl. Spectrosc. 58, 33–40.

Zhan, W., Bard, A.J., 2006. Anal. Chem. 78, 726–733.

Zoski, C.G., Liu, B., Bard, A.J., 2004. Anal. Chem. 76, 3646–3654.